Self-selecting vapor growth of transition-metal-halide single crystals

J.-Q. Yan* and M. A. McGuire
Materials Science and Technology Division, Oak Ridge National Laboratory, Oak Ridge, Tennessee 37831, USA

(Received 14 November 2022; accepted 9 January 2023; published 23 January 2023)

Transition-metal halides can host a large variety of novel phenomena, such as magnetism in the monolayer limit, quantum spin liquid and spiral spin liquid states, topological magnons, and chiral phonons. Sizable high-quality single crystals are necessary for investigations of magnetic and lattice excitations by, for example, inelastic neutron scattering. In this paper, we review a less well-known vapor transport technique, self-selecting vapor growth, and report our growths of transition-metal halides using this technique. We report the growth and characterizations of sizable single crystals of α-$RuCl_3$, $CrCl_3$, $Ru_{1-x}Cr_xCl_3$, and $CrBr_3$. In order to expedite the conversion of starting powder to single crystals, we modified the technique by cooling the growth ampoule through an appropriate temperature range. Our work shows that the self-selecting vapor transport technique can provide large single crystals of transition-metal halides, demonstrating its potential for providing high-quality single crystals of quantum materials.

DOI: 10.1103/PhysRevMaterials.7.013401

The study of materials confined to two spatial dimensions is associated with many hallmark discoveries and phenomena in condensed matter systems. The bulk of this experimental work is traditionally done using carefully grown and finely tuned thin films, but more recently cleavable, layered materials have provided a complementary top-down approach. Ultrathin flakes can be peeled from crystals comprising neutral layers joined to one another through van der Waals (vdW) bonding. This enables not only the study of two-dimensional (2D) physics in single materials, but also the construction of vdW heterostructures combining functionalities [1]. Transition-metal halides represent one important class of such vdW layered compounds [2]. These compounds often adopt structures that are relatively simple, yet contain interesting structural motifs like triangular or honeycomb networks. These materials appear over a wide breadth of current materials physics contexts, including 2D magnetic order [3], multiferroicity [4–7], quantum spin liquids [8,9], spiral spin liquids [10], topological magnons [11–13], and chiral phonons [14]. The availability of sizable, high-quality crystals of layered halides is important in enabling continued progress in these areas.

Often transition-metal halides can be grown by simple vapor transport or sublimation reactions [15,16] due to their high vapor pressure at elevated temperatures. This typically produces platelike crystals with lateral dimensions from 1 to 10 mm, but with thicknesses limited to between 0.001 and, in rare cases, 0.1 mm. Some examples melt congruently, and in those cases Bridgman growths can be a better approach [10]. While many 2D and device physics research applications require only small crystals to exfoliate, building the prerequisite detailed understanding of these materials often demands measurements on thicker crystals with larger mass and smaller aspect ratios. This is particularly true for neutron scattering techniques, which provide valuable information about the crystal and magnetic structures as well as lattice and magnetic excitations.

In this work, we review the principles of a less well-known vapor transport technique, self-selecting vapor growth (SSVG) [17], and report the growth and characterization of single crystals of transition-metal halides. This technique was developed about 50 years ago but has only been employed to grow II-VI and IV-VI semiconductors. We grew sizable single crystals of transition-metal halides using SSVG and found cooling through a temperature range is rather effective in expediting the conversion of the starting powder to crystals. This growth effort was motivated by the need of large single crystals to study the fractionalized excitations in the quantum spin liquid candidate α-$RuCl_3$ and bosonic Dirac physics in chromium halides (CrX_3, X = Cr, Br, and I) with ferromagnetic honeycomb layers. For all transition-metal halides mentioned in this work, conventional vapor transport growths using a large temperature gradient are used when small crystals are more appropriate for the planned experimental investigations.

I. SELF-SELECTING VAPOR TRANSPORT GROWTH

Crystal growth by vapor transport makes use of the vapor phase generated from chemical reaction between the starting materials and the transport agent in a chemical vapor transport (CVT) growth, or from sublimation or decomposition of starting materials in a physical vapor transport (PVT) growth. PVT growths can occur through different routes: Sublimation, decomposition sublimation, and autotransport [15]. In a sublimation growth, the solid at the source end sublimates and the vapor deposits at the sink end of the growth ampoule. In the case of a decomposition sublimation process, the solid at the source end decomposes into gaseous phases, then

*yanj@ornl.gov

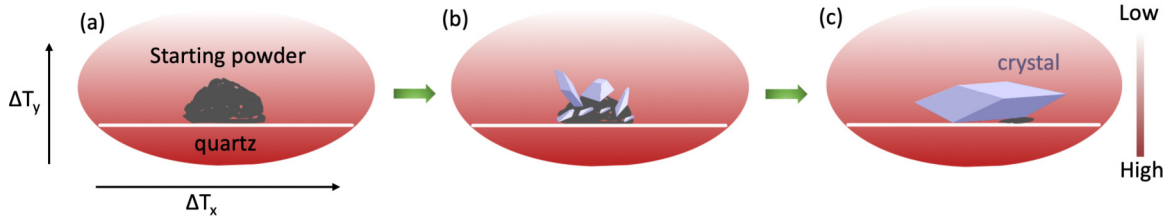

FIG. 1. Illustration of the self-selecting vapor transport growth performed inside of a sealed ampoule, normally a fused-quartz tube. (a) Starting powder in a well-defined temperature gradient. Only a small portion of the quartz tube is drawn for simplification. A small temperature gradient is applied along the vertical direction as illustrated by the color scale. A small horizontal temperature gradient can be also applied to help the grain selection. (b) Over time, part of the starting powder is converted to small crystals growing on top of the powder. (c) At the end of an ideal growth, one large single crystal forms consuming all starting powder as well as the smaller crystals that formed at the early stage of the growth.

crystals with the composition of the initial solid can precipitate at the sink end out of the gaseous phases. In the so-called autotransport growth, the gaseous phases resulting from the decomposition of the initial solid act as the transport agent. The PVT growth mechanism of each transition-metal halide varies depending on the composition, partial pressure, and role of the gaseous phases inside of the growth ampoule. More than one of these mechanisms may occur in a single growth, for example, for the PVT growth of $CrCl_3$ [15].

For most CVT and PVT growths, a large temperature gradient over, for example, 20°C is applied along the growth ampoule. This temperature gradient drives the mass transport that leads to the crystallization of the desired phase at the sink end. One natural result of this process is that the source powder and the resulting crystals stay at different ends of the growth ampoule and are separated from each other. This approach has been successfully employed to grow high-quality single crystals of various materials including intermetallics, oxides, transition-metal chalcogenides, and halides [15].

SSVG is one special vapor transport growth that occurs in a much smaller temperature gradient with the crystals growing on top of the starting powder. The principles and applicability of this technique are well reviewed previously [17]. Figure 1 illustrates the principles of a SSVG. The loosely packed starting powder was placed in a small (e.g., less than 2°C) but well-controlled temperature gradient illustrated in Fig. 1(a). SSVG can be performed in a horizontal configuration, which can have both horizontal and vertical temperature gradients, or a vertical configuration, which normally has a vertical temperature gradient only. As time goes by, crystals show up on top of the starting powder which is the coolest part of the powder. The term "self-selecting" comes from the fact that the growth of crystals on the cool top of the polycrystalline source favors the fastest growing orientations. Crystals continue to form and grow with the vapor transport of the hot source materials. Over time, one grows at the expense of the starting powder and the smaller grains that formed at the early stage of the growth; eventually one large single crystal is obtained [see Fig. 1(c)] in an ideal growth.

Compared to other vapor transport growths, SSVG is distinguished by the following features: (1) The small temperature gradient makes the growth nearly isothermal. This leads to exceptional compositional uniformity for solid solutions and is critical for systems where the distribution coefficient is temperature dependent. (2) Crystals grow on top of the starting powder which acts as a seed. There is no contact between the crystals and the growth ampoule or crucible. Thus the crystals are free of strain from the contact with the container.

SSVG can be a CVT process when transport agents are present or a PVT process otherwise. This technique has been employed to grow large crystals of semiconducting II-VI and IV-VI material systems. To the best of our knowledge, it has not been employed to grow other novel quantum materials. In this paper, we report the growth of large single crystals of α-$RuCl_3$, $CrCl_3$, $Ru_{1-x}Cr_xCl_3$, and $CrBr_3$ using SSVG. Previous growths of semiconducting II-VI and IV-VI materials were performed at a fixed setup temperature and the growths can be time-consuming. In order to expedite the self-selecting vapor transport growth of transition-metal halides, we modified the growths by cooling in an appropriate temperature range at a reasonably slow cooling rate which is more efficient in converting all the starting powder to one single crystal.

II. α-$RuCl_3$

α-$RuCl_3$ continues to be intensely studied as a candidate Kitaev spin liquid [18]. Inelastic neutron scattering is one of the few direct probes of the fractionalized excitations in quantum spin liquid materials, therefore, the availability of large single crystals is critical. This compound does not melt but sublimes at high temperatures. This indicates that growths using solidification from a molten state, such as Bridgman, Czochralski, and floating-zone techniques, are not applicable to the growth of α-$RuCl_3$ crystals. Instead, vapor transport should be an effective approach. In Table I of Ref. [19], Kim *et al.* summarized the vapor transport conditions reported in the literature. Single crystals of α-$RuCl_3$ can be grown in horizontal tube furnaces with a purposely controlled temperature gradient with the aid of a transport agent such as Cl_2 (730–660°C in Ref. [20], 750–650°C in Ref. [21]) or $TeCl_4$ (700–650°C in Ref. [16]) or even no transport agent since α-$RuCl_3$ has a reasonable vapor pressure at elevated temperatures. In these types of growths, the starting α-$RuCl_3$ powder is kept at the hotter end of the growth ampoule during the growth; platelike α-$RuCl_3$ crystals form at the cooler end after an extended stay at high temperatures. α-$RuCl_3$ crystals grown in this manner are normally plates with limited thickness.

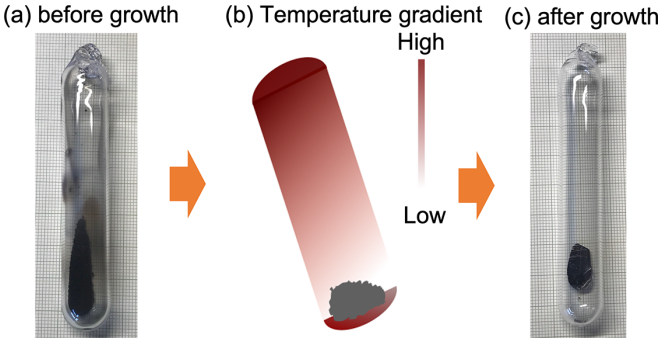

FIG. 2. Self-selecting vapor transport growth of α-$RuCl_3$. (a) About 1 g of α-$RuCl_3$ powder sealed in a fused quartz tube under vacuum. (b) The temperature gradient configuration used in our growths of all transition-metal halides mentioned in this work. Note both the vertical and lateral components near the powder. The ampoule can be tilted to any angle as needed (see Fig. 8) in addition to horizontal or vertical positions. Regardless of the tilting angle, the top of the ampoule should be kept at a temperature higher than that on top of the powder. (c) All starting powder is converted to one single crystal after growth. A millimeter-grid graph paper was used in panels (a) and (c). As discussed in the text, details of the temperature gradient and cooling rate control the shape and dimension of the resulting crystals.

We employ SSVG to grow α-$RuCl_3$ single crystals that are typically larger than 1 g per piece for inelastic neutron scattering (INS) measurements. These large single crystals with a small mosaic allow INS measurements without coaligning many smaller pieces. More importantly, by carefully controlling the temperature gradient around the powder, we can control the shape of resulting crystals as illustrated in Figs. 3(c) and 3(d). A slightly larger temperature gradient along the ampoule favors the growth of platelike crystals.

In the early stage of our work on this project, commercial α-$RuCl_3$ powder from Alfa Aesar was first purified before crystal growth or further studies [22]. In recent growths, two types of α-$RuCl_3$ powder are used. Most growths were performed using the commercial powder from Furuya Metals (Japan). Some growths were performed using α-$RuCl_3$ powder obtained from $AlCl_3$-KCl salt. The detailed procedure for producing α-$RuCl_3$ powder by reacting RuO_2 and $AlCl_3$-KCl salt was reported previously [23]. X-ray powder diffraction measurements found no impurity phases in either powder sample. Magnetic measurements show a magnetic ordering temperature of 14 K for the commercial powder and 12 K for the powder made from the salt flux. In the whole temperature range 2 K–300 K, the commercial powder has a larger magnetization.

The starting powder was sealed under dynamic vacuum in a fused quartz ampoule. For the growth of crystals about 1 g/piece, the fused-quartz tube used has an outer diameter of 19 mm, a wall thickness of 1.5 mm, and a length of approximately 100 mm. When the growth used 2 g or more of material, a tube with an outer diameter of 25 mm was used instead to avoid possible tube failure due to overpressure at high temperatures. The sealed ampoule was then put inside of a box furnace with a temperature gradient as shown in Fig. 2(b). The details of generating such a temperature gradient will be presented later. After dwelling at a furnace set point temperature of 1060°C for 6 h, the furnace was cooled to 800°C at 4°C/h. The furnace was then powered off to cool to room temperature. When the cooling rate is in the range 2–4°C/h, all of the powder inside of the ampoule converts into one single crystal. As shown in Figs. 3(d) and 3(e), the crystals are rather thick and look like Chinese style Go stones. Platelike crystals can be obtained by increasing the cooling rates or by increasing the temperature gradient along the quartz ampoule. These large crystals have a minimal amount of stacking faults and order antiferromagnetically at 7 K [24]. The semiquantitative elemental analysis on cleaved surfaces was performed using a Hitachi TM-3000 tabletop electron microscope equipped with a Bruker Quantax 70 energy-dispersive x-ray system. The energy-dispersive spectroscopy (EDS) measurement confirms the stoichiometry of the as-grown crystals. The crystal and magnetic structures in zero [24] and high magnetic fields [25] have been carefully characterized by single-crystal x-ray and neutron diffraction measurements. A structural transition from high temperature *C2/m* to low temperature *R*-3 occurs around 140 K upon cooling. Some pieces of large crystals have been used in INS experiments by our collaborators to

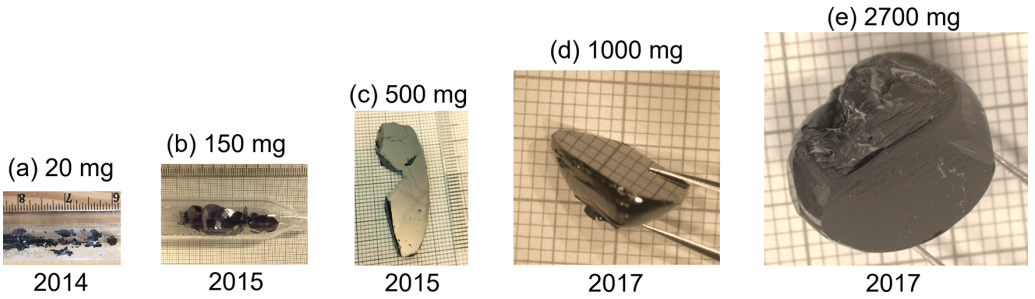

FIG. 3. α-$RuCl_3$ crystals grown at different stages of our work. (a) A conventional vapor transport growth performed in a horizontal tube furnace with a temperature gradient of about 45 °C between the starting powder at the hot end and crystals at the cold end. (b)–(e) Self-selecting vapor transport growths performed in a box furnace. The increasing crystal dimension results from a better control of the temperature gradient around the starting powder. The number beneath each panel shows in what year the growth was performed. The picture in panel (c) was taken by Arnab Banerjee. α-$RuCl_3$ powder purified by Craig Bridges at Oak Ridge National Laboratory was used for the growth of crystals in (a)–(c). Commercial α-$RuCl_3$ powder from Furuya Metals was used to grow the large crystals shown in (d) and (e). A millimeter-grid graph paper was used in (b)–(e).

investigate the magnetic and lattice excitations and to search for the fractionalized excitations with and without magnetic fields [26–29].

Kubota *et al.* reported the growth of α-$RuCl_3$ crystals using a Bridgman furnace [30]. In this growth, the growth ampoule was pulled downward in a Bridgman furnace at a rate of 3 mm/h over 80 h. This resembles the operation for a typical Bridgman growth out of melt. However, it should be noted that only solid and vapor phases are involved in the growth of α-$RuCl_3$ based on our understanding of the growth mechanism. This growth performed inside of a Bridgman furnace is still one type of vapor transport growth. In such a growth, the starting powder can be located at any position inside of the growth ampoule, often at the top (e.g., using the two-chamber technique as described in Ref. [16]) or the bottom end. Regardless of the position of the starting powder, as long as the crystals are found on top of the powder or where the powder is in case of a complete conversion of starting powder to crystals, this growth using a Bridgman-like setup is also a self-selecting vapor transport growth. In this case, the conversion of powder to crystal is controlled by the vertical temperature profile and the pulling rate. However, if the crystals grow at a different and cooler position of the ampoule and are separated from the starting powder, this growth can be understood as vapor transport growths performed inside of a tube furnace with a larger temperature gradient. The growth temperature gradient can be one important factor determining the crystal quality and properties. The recently discussed sample dependence of thermal transport properties indicates that the growth conditions can have a dramatic effect on the stoichiometry, layer stacking sequence, and structural defects, and hence the physical properties [31].

III. $CrCl_3$

Cr trihalides (CrX_3, X = Cl, Br, and I) with ferromagnetic honeycomb layers are model systems to study the magnonic Dirac physics [32]. Large single crystals are needed to study the bosonic excitations by, for example, INS. In order to grow high-quality $CrCl_3$ crystals, we first purified commercial $CrCl_3$ using a vapor transport reaction. The commercial $CrCl_3$ was first dried in dynamic vacuum overnight at room temperature, then sealed in a fused quartz tube with an outer diameter of 19 mm, a wall thickness of 1.5 mm, and a length of 150 mm. The sealed ampoule was put inside of a tube furnace with the hot end with dry $CrCl_3$ at 700°C and the cold end at 400 °C. A large amount of magenta-violet transparent $CrCl_3$ crystals were found at the cold end after 12 h. About 1 g of these small crystals were then transferred into a new quartz tube of the same diameter but only 100 mm long. The sealed ampoule was put inside of a box furnace and heated to 950°C, held at this temperature for 2 h and then cooled down to 600°C at 3°C/h. The furnace was then turned off to cool to room temperature. Figure 4(a) shows the growth ampoule after growth. Occasionally some white residue can be found at the bottom of the growth ampoule. EDS and x-ray powder diffraction measurements confirm this is amorphous silica resulting from the reaction of residual moisture, $CrCl_3$, and the quartz tube. In the extreme situation, green colored Cr_2O_3 might show up inside of the growth ampoule, which

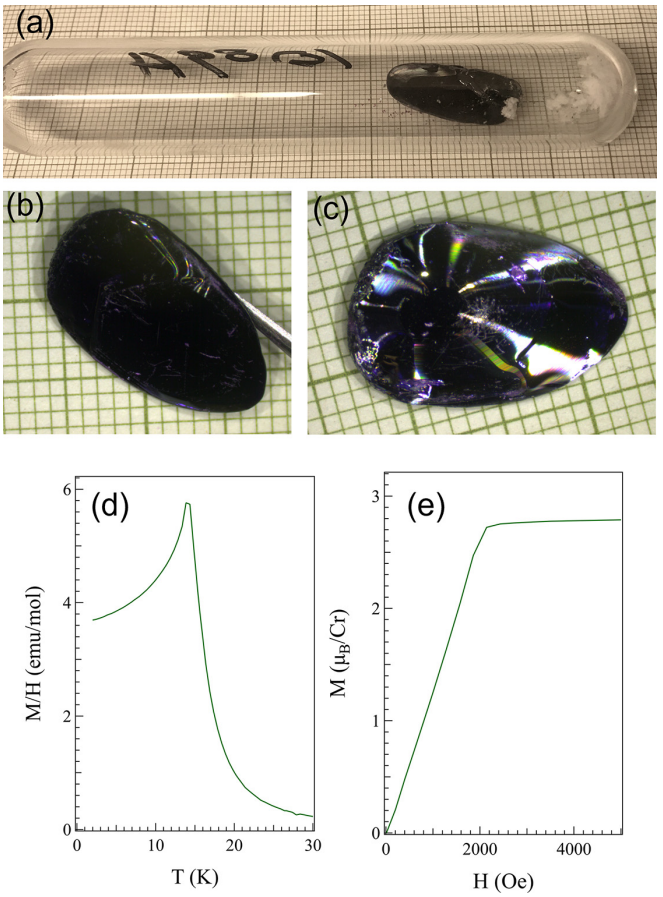

FIG. 4. (a) Picture of one $CrCl_3$ crystal of 1.2 g inside of the growth ampoule on a millimeter grid. The white fluffy material at the bottom of the ampoule is amorphous SiO_2 resulting from the reaction between residual moisture, $CrCl_3$, and the quartz tube as described in the text. (b), (c) A closer view of both sides of the Go-stone-like crystal. (d) Temperature dependence of magnetization in a magnetic field of 100 Oe applied along the *ab* plane. (e) In-plane field dependence of magnetization at 2 K.

is a good indication of water contamination coming from either the starting materials or the growth ampoule. Using well-dried starting materials as described above would significantly reduce the amount of these secondary phases in the products. Just like the growth of α-$RuCl_3$ described above, $CrCl_3$ crystals grown in this manner can be rather thick with a shape of a single Go stone. Figures 4(b) and 4(c) show a closer view of both sides of the crystal. EDS confirms the stoichiometry of $CrCl_{3.0(1)}$. Magnetic measurements [see Figs. 4(d) and 4(e)] confirm $CrCl_3$ crystals grown by SSVG show the same magnetic properties as those thin crystals grown by conventional vapor transport technique [33]. The temperature dependence of magnetization in the paramagnetic state (not shown) shows a structure transition around 250 K as reported previously [33].

One piece of $CrCl_3$ crystal of 0.88 g grown by SSVG technique was used in INS studies of the topological magnons and phonons [13,34]. The mosaic of this crystal is smaller than 0.68°, much smaller than that of coaligned crystals which is normally several degrees. This small mosaic turns out to

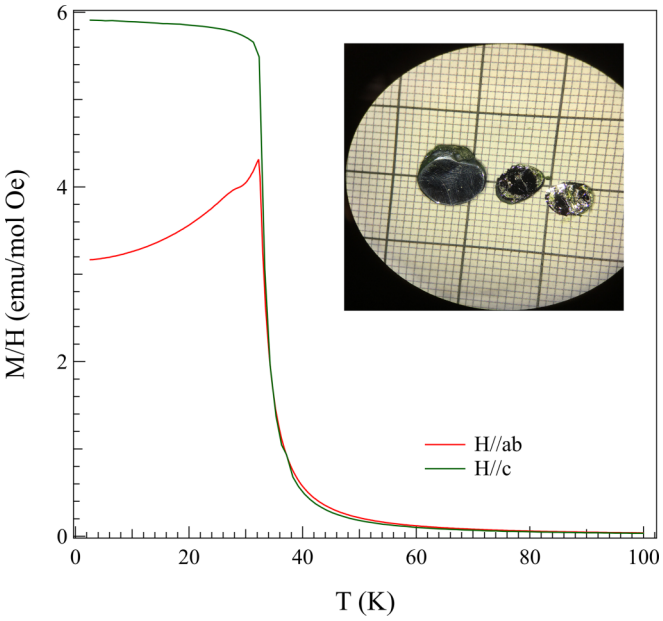

FIG. 5. Temperature dependence of magnetization measured in a field cool mode using an applied magnetic field of 100 Oe. Inset shows a photograph of the $CrBr_3$ crystals on a millimeter grid, with the smaller of the two cleaved into two (center and right).

be important to accurately determine the gaps in topological magnon spectra [13].

IV. $CrBr_3$

$CrBr_3$ powder used for the crystal growth was synthesized by reacting Cr powder with bromine produced by decomposition of $CuBr_2$. One of us developed this double chamber reaction ampoule specifically for this and similar growths. The details for this synthesis were reported previously [16]. About 0.8 g of $CrBr_3$ powder was sealed in a fused quartz tube with an outer diameter of 19 mm, a wall thickness of 1.5 mm, and a length of 100 mm. The sealed ampoule was put inside of a box furnace and heated to 950°C, held at this temperature for 6 h and then cooled down to 600°C at 2°C/h. The furnace was then powered off to cool to room temperature. This procedure enables a full conversion of all starting powder into two single crystals (along with some green residue). The inset of Fig. 5 shows the intact larger crystal and the smaller crystal cleaved in two. The composition determined by EDS on cleaved surfaces is $CrBr_{3.2(1)}$. Figure 5 shows the anisotropic temperature dependence of magnetization measured in an applied magnetic field of 100 Oe. The magnetic ordering temperature is 33 K, consistent with previous results [35].

V. $Ru_{1-x}Cr_xCl_3$

In addition to high pressure and high magnetic field, chemical substitution [36–38] is an effective approach to manipulating the magnetic ground state and competing interactions in α-$RuCl_3$. The growth of large single crystals of doped α-$RuCl_3$ is rather challenging mainly because the dopant can have a quite different vapor pressure than the parent compound. Here we use $Ru_{0.9}Cr_{0.1}Cl_3$ as an

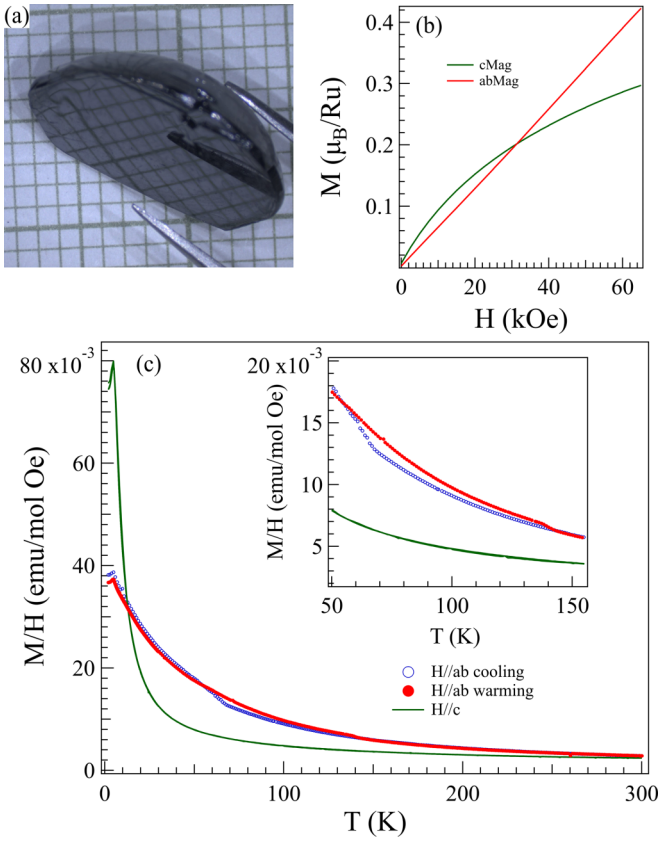

FIG. 6. (a) $Ru_{1-x}Cr_xCl_3$ crystals on a millimeter grid. (b) Field dependence of magnetization at 2 K. (c) Temperature dependence of magnetic susceptibility measured in an applied magnetic field of 1 kOe. Inset highlights the loop induced by the first-order structural transition.

example to demonstrate that large single crystals of uniform solid solutions of transition-metal halides can be obtained by SSVG possibly due to the small temperature gradient. To grow Cr-substituted α-$RuCl_3$, sublimation cleaned small $CrCl_3$ crystals and well-dried α-$RuCl_3$ powder obtained from $AlCl_3$-KCl salt were used as the starting materials. A mixture of $CrCl_3$ crystals and α-$RuCl_3$ powder in the molar ratio of 1:9 was sealed in a fused-quartz tube with an outer diameter of 19 mm, a wall thickness of 1.5 mm, and a length of 100 mm. The same growth parameters as those for α-$RuCl_3$ were used for the growth of lightly doped compositions. Figure 6(a) shows the picture of one $Ru_{0.9}Cr_{0.1}Cl_3$ crystal. A portion of the crystal was carefully removed and used for the magnetic measurements and elemental analyses. The Ru/Cr ratio was confirmed by EDS on different cleaved surfaces. We found no significant variation in Cr concentration laterally across cleaved surfaces or through the thickness of the crystal comparing different cleaved surfaces. Figure 7 shows the (0 0 *l*) reflections collected by x-ray diffraction from cleaved surfaces. (0 0 *l*) reflections for other compounds mentioned in this work are also shown for comparison. The layer spacing, *d*, of $Ru_{0.9}Cr_{0.1}Cl_3$ is slightly larger than that of α-$RuCl_3$ but smaller than that of $CrCl_3$. The composition dependence of layer spacing follows Vegard's law. Figure 6(b) shows the field dependence of magnetization measured with the field

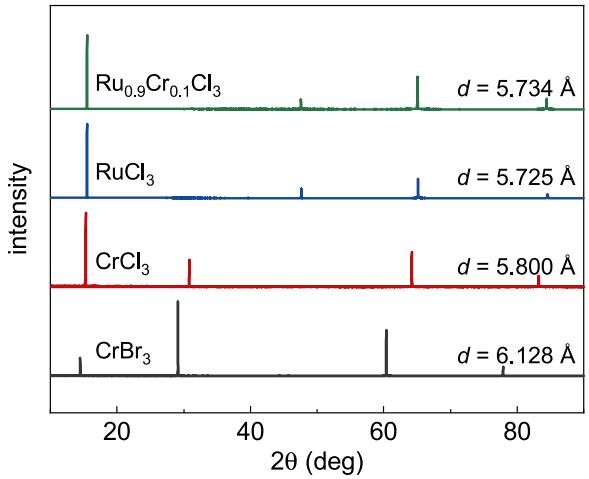

FIG. 7. (0 0 l) reflections of all compounds mentioned in this work collected on cleaved surfaces by x-ray diffraction. Also listed in the figure is the layer spacing, d, which is independent of the layer stacking.

applied perpendicular and parallel to the ab plane. A linear field dependence is observed when the magnetic field is applied parallel to the ab plane. This is in contrast to a nonlinear field dependence when the field is perpendicular to the ab plane. Figure 6(c) shows the temperature dependence of magnetization. With 10% of Ru substituted by Cr, the magnetic ordering temperature is suppressed from 7 K in α-$RuCl_3$ to near 5 K in $Ru_{0.9}Cr_{0.1}Cl_3$. We observed only one anomaly around 5 K which indicates the absence of stacking faults [24]. The doping dependence of magnetic ordering temperature agrees with previous reports [36,39]. Thermally hysteretic behavior is seen in the temperature range 70 –140 K when the magnetic field is parallel to the ab plane, likely associated with the first-order structural phase transition [24]. Compared to that in α-$RuCl_3$, the structural transition occurs in a wider temperature range. The structure transition in $CrCl_3$ occurs around 250 K, which is about 100 K higher than that in α-$RuCl_3$. It would be interesting to monitor how the structure transition evolves with the substitution in $Ru_{1-x}Cr_xCl_3$. We also studied a couple of crystals with less Cr substitution. For these lightly doped compositions, the Ru/Cr ratio determined from EDS agrees with that in the starting materials. Whether this ideal behavior persists with more Cr substitution deserves further study.

VI. DISCUSSION

One unique feature of SSVG is the unusually small temperature gradient applied vertically and/or horizontally to the starting powder. However, in reality, it is rather challenging to obtain such a small but reproducible temperature gradient. The years labeling the crystal pictures in Fig. 2 show how long it took for us to gradually get a good understanding and control of the ideal temperature gradient for the growth of large α-$RuCl_3$ crystals even though we realized its importance at the early stage of the work. Such a small temperature gradient can be obtained in either a tube furnace or a box furnace. We tested SSVGs using both one-zone and two-zone tube furnaces and

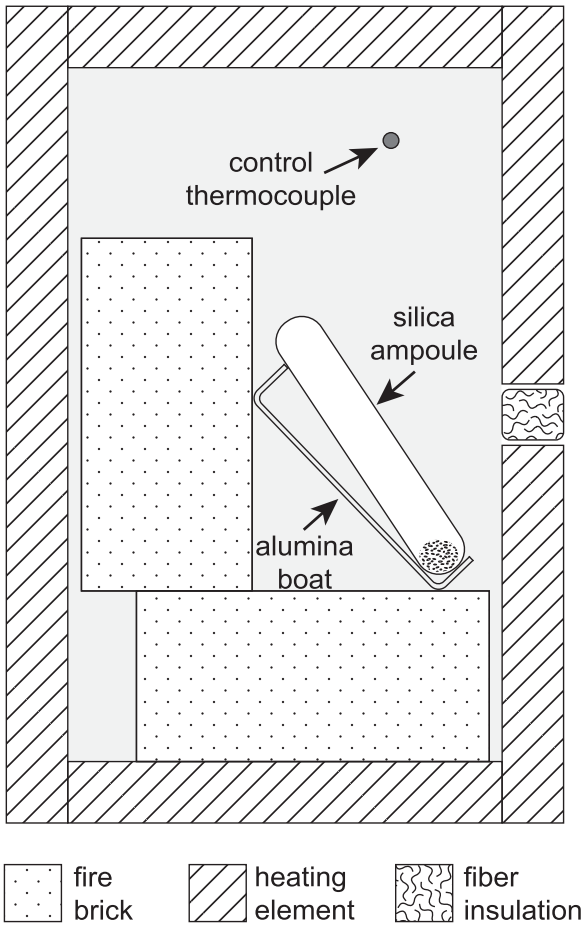

FIG. 8. Schematic picture of the furnace that we used to grow all transition-metal halides and chalcogenides mentioned in this work. The amount of fiber insulation inside of the vent hole helps create the desired temperature gradient near the bottom end of the growth ampoule.

obtained some beautiful crystals. However, we found that it is difficult to control the vertical temperature gradient. We thus performed the growths in a box furnace making good use of the natural temperature gradient of the furnace. The temperature inside of a box furnace is not uniform and it is rather challenging to measure the temperature variation at different positions inside of the furnace. The consequence of this is that we do not know the exact temperature gradient near the powder. However, it is expected to be rather small.

Figure 8 shows how Al_2O_3 fire bricks and fiber insulation are employed inside of a box furnace to create a desired temperature gradient near the bottom of the growth ampoule. This figure shows a cross-sectional sketch of a Thermolyne muffle furnace from Thermo Scientific (model F6038CM), which has been rotated to sit on its side, placing the vent hole (usually on the top of the furnace) on the right-hand side. There is a natural vertical temperature gradient due in part to convection. The amount of fiber insulation inside of the vent hole can be adjusted to control the temperature gradient nearby. We identified the position best for SSVG by varying the location of the ampoule with respect to the furnace door and with respect to the furnace vent. We noticed that crystals always

appear at the coldest place of the ampoule, which is a good indicator of the detailed temperature profile. When there is a temperature gradient larger than what is required for a SSVG and the starting powder stays at a hot place, crystals form at a position away from the starting powder and often have a few large grains. Changes in the crystal growth resulting from small changes in the placement of the ampoule in the furnaces suggest the detailed temperature gradient near the powder has a dominant effect on the shape of the grown crystals. Once an ideal position was located, we tried to place the growth ampoule at the same position in every growth. It should be noted that our growths have been reproduced in several different box furnaces although the temperature distribution in each furnace can be different. We also tested growths by positioning the ampoule upright inside of an Al_2O_3 crucible and filling the space between the growth ampoule and the Al_2O_3 crucible with fiber insulations. In such kind of growths without any temperature gradient around the starting powder, many pieces of platelike crystals are normally obtained. Occasionally, we obtained nice crystals by keeping the growth ampoule upright inside of an alumina crucible without any fire insulations around the growth ampoule. In this case, the horizontal temperature gradient is negligible and mainly the vertical temperature gradient drives the growth.

Cooling at an appropriate rate obviously promotes the transformation from powder to crystals in a SSVG. We tried the growth of α-$RuCl_3$ at 1000°C and 900°C in the temperature gradient optimized for SSVG. The crystallization is not complete even after a month, versus only 3–4 days when an appropriate cooling rate is used. After confirming the importance of cooling during the crystallization, we further tested how the cooling rate affects the shape and size of crystals. All test growths were performed using a 1 g batch. If the cooling rate is above 8°C/h, some powder remains inside of the growth ampoule and several pieces of crystals are normally found. One single crystal is normally observed if the cooling rate is lower than 4°C/h. For growths with a cooling rate in the range of 4–8°C/h, either one piece of crystal with large in-plane dimension or a few pieces with some smaller in-plane dimension typically result. The above knowledge learned from the growth of α-$RuCl_3$ worked well for other transition-metal halides mentioned in this work. We thus choose different cooling rates depending on the crystal geometry desired for specific measurements.

Two experimental observations indicate that the total pressure inside of the growth ampoule affects the nucleation and growth. We tried SSVG of $MoCl_3$, CrI_3, and $Os_{0.55}Cl_2$ but the conversion of powder to crystal is never complete and we obtained only millimeter-sized single crystals even with a slow cooling rate of 1°/h [8,40]. All three compounds have a high vapor pressure even at temperatures below 500°C. The high vapor pressure might promote nucleation. An even longer stay at relatively low temperatures might be desired. The other experimental observation indicating the detrimental effects of high pressure is that high-purity starting materials facilitate the growth of large single crystals. Some commercial chemicals are not pure and may have volatile impurities. Full conversion of starting powder to crystals is normally observed after purifying the commercial starting materials. This motivates us to purify, for example, $CrCl_3$, before crystal growth as described above. Also for the same reason, in some growths of α-$RuCl_3$, we used high-purity powders synthesized by reacting RuO_2 with $AlCl_3$-KCl [23]. For materials with high vapor pressure the growth temperature should be kept relatively low, which may also require a slower cooling rate and overall longer reaction time to allow complete reaction.

SSVG should be adaptable to grow quantum materials other than transition-metal halides presented in this work and II-VI and IV-VI semiconductors reported in literature. Recently, vapor transport growth in a small temperature gradient was employed to grow the intrinsic antiferromagnetic topological insulator $MnBi_2Te_4$ and related compounds [41,42]. Motivated by this, we tried the SSVG of $MnBi_2Te_4$. Submillimeter-sized crystalline plates are obtained on top of the starting powder after dwelling at 565°C for over 3 wk. More growths and characterizations are in progress to investigate whether SSVG can provide a better control than flux growth [43] and chemical vapor transport [41] of the lattice defects, which are believed to play an essential role in realizing the elusive quantum anomalous Hall effect in $MnBi_2Te_4$ [44]. We also tested the SSVG of $MoSe_2$ and WSe_2 in the presence of I_2 and obtained millimeter-sized crystals by keeping the growth ampoule at 1025°C for over a month. These preliminary growths suggest that SSVG can be employed to grow other quantum materials.

VII. SUMMARY

In summary, we review the self-selecting vapor growth technique. This technique was developed over a half century ago, but its application has been limited to the II-VI and IV-VI semiconductors. We report the growth of large single crystals of transition-metal halides using this technique. We performed the SSVG by cooling through a temperature range which has been proved to expedite the conversion of the starting powder to crystals. The temperature range ideal for the growth is determined by the vapor pressure of the starting materials. An ideal vapor pressure should be high enough to allow efficient material conversion but low enough to control the number of resulting crystals. A slower cooling rate is favored for a complete conversion of the starting powder to one single large crystal. Preliminary growths on transition-metal chalcogenides suggest that this technique works well for other quantum materials.

ACKNOWLEDGMENTS

The authors acknowledge collaborations and discussions with A. Banerjee, C. Bridges, H. Cao, A. Christianson, S. Do, S. Gao, P. Kelley, D. Mandrus, A. May, S. Nagler, B. Sales, and A. Tennant. This work was supported by the U.S. Department of Energy, Office of Science, Basic Energy Sciences, Materials Sciences and Engineering Division. Crystal growth of $RuCl_3$ after 2020 was supported by the U.S. Department of Energy, Office of Science, National Quantum Information Science Research Centers, Quantum Science Center.

[1] A. K. Geim and I. V. Grigorieva, Van der Waals heterostructures, Nature (London) **499**, 419 (2013).

[2] M. A. McGuire, Crystal and magnetic structures in layered, transition metal dihalides and trihalides, Crystals **7**, 121 (2017).

[3] B. Huang, G. Clark, E. Navarro-Moratalla, D. R. Klein, R. Cheng, K. L. Seyler, D. Zhong, E. Schmidgall, M. A. McGuire, D. H. Cobden *et al.*, Layer-dependent ferromagnetism in a van der Waals crystal down to the monolayer limit, Nature (London) **546**, 270 (2017).

[4] T. Kurumaji, S. Seki, S. Ishiwata, H. Murakawa, Y. Kaneko, and Y. Tokura, Magnetoelectric responses induced by domain rearrangement and spin structural change in triangular-lattice helimagnets NiI_2 and CoI_2, Phys. Rev. B **87**, 014429 (2013).

[5] X. Wu, Y. Cai, Q. Xie, H. Weng, H. Fan, and J. Hu, Magnetic ordering and multiferroicity in MnI_2, Phys. Rev. B **86**, 134413 (2012).

[6] T. Kurumaji, S. Seki, S. Ishiwata, H. Murakawa, Y. Tokunaga, Y. Kaneko, and Y. Tokura, Magnetic-Field Induced Competition of Two Multiferroic Orders in a Triangular-Lattice Helimagnet MnI_2, Phys. Rev. Lett. **106**, 167206 (2011).

[7] Y. Tokunaga, D. Okuyama, T. Kurumaji, T. Arima, H. Nakao, Y. Murakami, Y. Taguchi, and Y. Tokura, Multiferroicity in $NiBr_2$ with long-wavelength cycloidal spin structure on a triangular lattice, Phys. Rev. B **84**, 060406(R) (2011).

[8] M. A. McGuire, Q. Zheng, J. Yan, and B. C. Sales, Chemical disorder and spin-liquid-like magnetism in the van der Waals layered 5*d* transition metal halide $Os_{0.55}Cl_2$, Phys. Rev. B **99**, 214402 (2019).

[9] K. W. Plumb, J. P. Clancy, L. J. Sandilands, V. V. Shankar, Y. F. Hu, K. S. Burch, H.-Y. Kee, and Y.-J. Kim, $\alpha - RuCl_3$: A spin-orbit assisted Mott insulator on a honeycomb lattice, Phys. Rev. B **90**, 041112(R) (2014).

[10] S. Gao, M. A. McGuire, Y. Liu, D. L. Abernathy, C. dela Cruz, M. Frontzek, M. B. Stone, and A. D. Christianson, Spiral Spin Liquid on a Honeycomb Lattice, Phys. Rev. Lett. **128**, 227201 (2022).

[11] L. Chen, J.-H. Chung, B. Gao, T. Chen, M. B. Stone, A. I. Kolesnikov, Q. Huang, and P. Dai, Topological Spin Excitations in Honeycomb FerromagnetCrI_3, Phys. Rev. X **8**, 041028 (2018).

[12] J. A. Schneeloch, Y. Tao, Y. Cheng, L. Daemen, G. Xu, Q. Zhang, and D. Louca, Gapless Dirac magnons in $CrCl_3$, npj Quantum Mater. **7**, 66 (2022).

[13] S.-H. Do, J. A. M. Paddison, G. Sala, T. J. Williams, K. Kaneko, K. Kuwahara, A. F. May, J. Yan, M. A. McGuire, M. B. Stone *et al.*, Gaps in topological magnon spectra: Intrinsic vs extrinsic effects, Phys. Rev. B **106**, L060408 (2022).

[14] T. Yin, K. A. Ulman, S. Liu, A. Granados del Águila, Y. Huang, L. Zhang, M. Serra, D. Sedmidubsky, Z. Sofer, S. Y. Quek *et al.*, Chiral phonons and giant magneto-optical effect in $CrBr_3$ 2D magnet, Adv. Mater. **33**, 2101618 (2021).

[15] M. Binnewies, R. Glaum, M. Schmidt, and P. Schmidt, *Chemical Vapor Transport Reactions* (De Gruyter, Berlin, 2012).

[16] A. F. May, J. Yan, and M. A. McGuire, A practical guide for crystal growth of van der Waals layered materials, J. Appl. Phys. **128**, 051101 (2020).

[17] A. Szczerbakow and K. Durose, Self-selecting vapour growth of bulk crystals—Principles and applicability, Prog. Cryst. Growth Charact. Mater. **51**, 81 (2005).

[18] H. Takagi, T. Takayama, G. Jackeli, G. Khaliullin, and S. E. Nagler, Concept and realization of Kitaev quantum spin liquids, Nat. Rev. Phys. **1**, 264 (2019).

[19] S. Kim, B. Yuan, and Y.-J. Kim, α-$RuCl_3$ and other Kitaev materials, APL Mater. **10**, 080903 (2022).

[20] M. Majumder, M. Schmidt, H. Rosner, A. A. Tsirlin, H. Yasuoka, and M. Baenitz, Anisotropic $Ru^{3+}4d^5$ magnetism in the $\alpha - RuCl_3$ honeycomb system: Susceptibility, specific heat, and zero-field NMR, Phys. Rev. B **91**, 180401(R) (2015).

[21] R. Hentrich, A. U. B. Wolter, X. Zotos, W. Brenig, D. Nowak, A. Isaeva, T. Doert, A. Banerjee, P. Lampen-Kelley, D. G. Mandrus, S. E. Nagler, J. Sears, Y. J. Kim, B. Buchner, and C. Hess, Unusual Phonon Heat Transport in $\alpha - RuCl_3$: Strong Spin-Phonon Scattering and Field-Induced Spin Gap, Phys. Rev. Lett. **120**, 117204 (2018).

[22] A. Banerjee, C. A. Bridges, J.-Q. Yan, A. A. Aczel, L. Li, M. B. Stone, G. E. Granroth, M. D. Lumsden, Y. Yiu, J. Knolle *et al.*, Proximate Kitaev quantum spin liquid behaviour in a honeycomb magnet, Nat. Mater. **15**, 733 (2016).

[23] J.-Q. Yan, B. C. Sales, M. A. Susner, and M. A. Mcguire, Flux growth in a horizontal configuration: An analog to vapor transport growth, Phys. Rev. Mater. **1**, 023402 (2017).

[24] H. B. Cao, A. Banerjee, J.-Q. Yan, C. A. Bridges, M. D. Lumsden, D. G. Mandrus, D. A. Tennant, B. C. Chakoumakos, and S. E. Nagler, Low-temperature crystal and magnetic structure of $\alpha - RuCl_3$, Phys. Rev. B **93**, 134423 (2016).

[25] C. Balz, L. Janssen, P. Lampen-Kelley, A. Banerjee, Y. H. Liu, J.-Q. Yan, D. G. Mandrus, M. Vojta, and S. E. Nagler, Field-induced intermediate ordered phase and anisotropic interlayer interactions in $\alpha - RuCl_3$, Phys. Rev. B **103**, 174417 (2021).

[26] A. Banerjee, P. Lampen-Kelley, J. Knolle, C. Balz, A. A. Aczel, B. Winn, Y. Liu, D. Pajerowski, J. Yan, C. A. Bridges *et al.*, Excitations in the field-induced quantum spin liquid state of $\alpha - RuCl_3$, npj Quantum Mater. **3**, 8 (2018).

[27] A. Banerjee, J. Yan, J. Knolle, C. A. Bridges, M. B. Stone, M. D. Lumsden, D. G. Mandrus, D. A. Tennant, R. Moessner, and S. E. Nagler, Neutron scattering in the proximate quantum spin liquid α-$RuCl_3$, Science **356**, 1055 (2017).

[28] C. Balz, P. Lampen-Kelley, A. Banerjee, J. Yan, Z. Lu, X. Hu, S. M. Yadav, Y. Takano, Y. Liu, D. A. Tennant, M. D. Lumsden, D. Mandrus, and S. E. Nagler, Finite field regime for a quantum spin liquid in α-$RuCl_3$, Phys. Rev. B **100**, 060405(R) (2019).

[29] S. Mu, K. D. Dixit, X. Wang, D. L. Abernathy, H. Cao, S. E. Nagler, J. Yan, P. Lampen-Kelley, D. Mandrus, C. A. Polanco, L. Liang, G. B. Halasz, Y. Cheng, A. Banerjee, and T. Berlijn, Role of the third dimension in searching for Majorana fermions in α-$RuCl_3$ via phonons, Phys. Rev. Res. **4**, 013067 (2022).

[30] Y. Kubota, H. Tanaka, T. Ono, Y. Narumi, and K. Kindo, Successive magnetic phase transitions in α-RuCl $_3$: XY-like frustrated magnet on the honeycomb lattice, Phys. Rev. B **91**, 094422 (2015).

[31] P. Lee, Quantized (or not quantized) thermal Hall effect and oscillations in the thermal conductivity in the Kitaev spin liquid candidate $RuCl_3$, Journal Club for Condensed Matter Physics, (2021).

[32] S. S. Pershoguba, S. Banerjee, J. Lashley, J. Park, H. Ågren, G. Aeppli, and A. V. Balatsky, Dirac Magnons in Honeycomb Ferromagnets, Phys. Rev. X **8**, 011010 (2018).

[33] M. A. McGuire, G. Clark, S. KC, W. M. Chance, G. E. Jellison, Jr., V. R. Cooper, X. Xu, and B. C. Sales, Magnetic behavior and

spin-lattice coupling in cleavable van der Waals layered $CrCl_3$ crystals, Phys. Rev. Mater. **1**, 014001 (2017).

[34] X. Li, S.-H. Do, J. Yan, M. A. McGuire, G. E. Granroth, S. Mu, T. Berlijn, V. R. Cooper, A. D. Christianson, and L. Lindsay, Phonons and phase symmetries in bulk $CrCl_3$ from scattering measurements and theory, Acta Mater. **241**, 118390 (2022).

[35] X. Yu, X. Zhang, Q. Shi, S. Tian, H. Lei, K. Xu, and H. Hosono, Large magnetocaloric effect in van der Waals crystal $CrBr_3$, Front. Phys. **14**, 43501 (2019).

[36] G. Bastien, M. Roslova, M. H. Haghighi, K. Mehlawat, J. Hunger, A. Isaeva, T. Doert, M. Vojta, B. Büchner, and A. U. B. Wolter, Spin-glass state and reversed magnetic anisotropy induced by Cr doping in the Kitaev magnet α- $RuCl_3$, Phys. Rev. B **99**, 214410 (2019).

[37] S.-H. Do, W.-J. Lee, S. Lee, Y. S. Choi, K.-J. Lee, D. I. Gorbunov, J. Wosnitza, B. J. Suh, and K.-Y. Choi, Short-range quasistatic order and critical spin correlations in $\alpha - Ru_{1-x}Ir_xCl_3$, Phys. Rev. B **98**, 014407 (2018).

[38] P. Lampen-Kelley, A. Banerjee, A. A. Aczel, H. B. Cao, M. B. Stone, C. A. Bridges, J.-Q. Yan, S. E. Nagler, and D. Mandrus, Destabilization of Magnetic Order in a Dilute Kitaev Spin Liquid Candidate, Phys. Rev. Lett. **119**, 237203 (2017).

[39] M. Roslova, J. Hunger, G. Bastien, D. Pohl, H. M. Haghighi, A. U. B. Wolter, A. Isaeva, U. Schwarz, B. Rellinghaus, K. Nielsch *et al.*, Detuning the honeycomb of the α-$RuCl_3$ Kitaev lattice: A case of Cr^{3+} dopant, Inorg. Chem. **58**, 6659 (2019).

[40] M. A. McGuire, J. Yan, P. Lampen-Kelley, A. F. May, V. R. Cooper, L. Lindsay, A. Puretzky, L. Liang, S. KC, E. Cakmak, S. Calder, and B. C. Sales, High-temperature magnetostructural transition in van der Waals-layered $\alpha - MoCl_3$, Phys. Rev. Mater. **1**, 064001 (2017).

[41] J-Q Yan, Z. Huang, W. Wu, and A. F. May, Vapor transport growth of $MnBi_2Te_4$ and related compounds, J. Alloys Compd. **906**, 164327 (2022).

[42] C. Hu, A. Gao, B. S. Berggren, H. Li, R. Kurleto, D. Narayan, I. Zeljkovic, D. Dessau, S. Xu, and N. Ni, Growth, characterization, and Chern insulator state in $MnBi_2Te_4$ via the chemical vapor transport method, Phys. Rev. Mater. **5**, 124206 (2021).

[43] J.-Q. Yan, Q. Zhang, T. Heitmann, Z. Huang, K. Y. Chen, J.-G. Cheng, W. Wu, D. Vaknin, B. C. Sales, and R. J. McQueeney, Crystal growth and magnetic structure of $MnBi_2Te_4$, Phys. Rev. Mater. **3**, 064202 (2019).

[44] J.-Q. Yan, Perspective—The elusive quantum anomalous Hall effect in $MnBi_2Te_4$: Materials, ECS J. Solid State Sci. Technol. **11**, 063007 (2022).